JOURNAL OF MATERIALS SCIENCE **36** (2001) 5779–5787

AC conductivity of nanostructured nickel oxide

V. BIJU, M. ABDUL KHADAR
Department of Physics, University of Kerala, Thiruvananthapuram 695 581, Kerala, India
E-mail: makhadar@mail.com

AC conductivity of consolidated nanoparticles of NiO, having different average particle sizes (2.5 nm–17 nm) was measured in the temperature range 313 K to 413 K and over the frequency range 50 Hz to 3 MHz. The ac conductivity of the samples was found to be enhanced by six to eight orders of magnitude over that of NiO single crystals reported in the literature. This large enhancement in conductivity is attributed to the high density of Ni^{2+} vacancies in the nanoparticles. The variation of ac conductivity with frequency of the applied signal and temperature is discussed on the basis of the Correlated Barrier Hopping (CBH) Model. The observed spread in activation energy and slope of the log σ_{ac} Vs log ω plots is attributed to the distribution of the charge carrier hopping distance and localization energies in the nanoparticle samples. The effect of the interfacial region on the electrical conductivity of the samples is analyzed by taking into account the contributions due to grain boundaries and triple junctions. The observed variation of measured ac conductivity with average particle size is semi-quantitatively explained based on the reasoning that the role of the triple junctions is to reduce the conductivity.

1. Introduction

Nanostructured materials are known to exhibit profoundly varied electrical properties in comparison to those of single crystals, polycrystals, glasses and thin films with the same average chemical composition. These variations in the electrical properties is a result of band structure modification due to spatial modulation of the lattice, quantum confinement of charge carriers, and dominant contributions from largely defective and strained grain boundaries in nanostructures [1–11].

NiO having a very low electrical conductivity of less than 10^{-13} $ohm^{-1}cm^{-1}$ at room temperature is classified as a 'Mott-Hubbard Insulator' [12–28]. However, introduction of Ni^{2+} vacancies and/or doping with monovalent cations like Li^{+} is reported to cause considerable increase in the conductivity [12–28]. Though NiO is perhaps the most extensively and carefully studied narrow band transition metal oxide in the form of single crystals, coarse-grained polycrystals and thin films, a complete theory of the conductivity mechanisms involved has not yet evolved [11–37]. Further, studies on the electrical properties of nanostructured NiO are very limited [38, 39]. The ac conductivity of NiO nanoparticles is expected to be significantly influenced by the volume fraction, thickness, continuity and degree of heterogeneity of grain boundaries. In the realm of nanostructured materials, the dependence of conductivity on the average particle size is most important and interesting. The present article reports a detailed analysis of the ac conductivity of NiO nanoparticles consolidated in the form of pellets as a function of temperature, frequency of the applied signal and average particle size.

2. Experimental

NiO nanoparticles were prepared through a two step process. In the first step, nanoparticles of nickel carbonate were prepared by arrested chemical precipitation. Nickel nitrate and ammonium carbonate were the starting materials and ethylenedinitrilotetraacetic acid disodium salt (dihydrate) EDTA was used as the stabilizer. All the chemicals used were of analytical grade. NiO nanoparticles were obtained by air annealing of the carbonate precursor at 523 K. The decomposition temperature was chosen after carrying out TGA analysis of the carbonate precursor. NiO nanoparticles having different average particle sizes were obtained by air annealing of the samples at higher temperatures [38].

The X-ray diffraction patterns of the samples are shown in Fig. 1. The average size of the particles were calculated from the line broadening of the X-ray diffraction peaks, corrected for instrumental broadening, using Scherrere's equation [40]. Details of annealing procedure and particle sizes are listed in Table I. The electron diffraction pattern of the sample, N1 having an average particle size of 2–3 nm is shown in Fig. 2. The diffused nature of the electron diffraction pattern is attributed to the contribution from the highly disordered grain boundaries of the nanoparticles.

The nanoparticle samples were consolidated in the form of cylindrical pellets having a diameter of 13 mm and thickness of about 1 mm by applying a uniaxial force of 4 tons for two minutes using a hydraulic press. Extreme care was taken to see that the pelletisation of all the samples were done under identical conditions. Conducting silver epoxy was applied on both the faces of the pellets to serve as electrodes. The pellets were first air dried for 30 minutes and then heat treated at

TABLE I Details of NiO nanoparticle samples

Sample code	Annealing temperature (K)	Duration (hrs)	Average particle size (nm)
N1	523	1	2–3
N2	573	1	4–5
N3	623	1	5–7
N4	723	1	12–13
N5	773	1	16–17

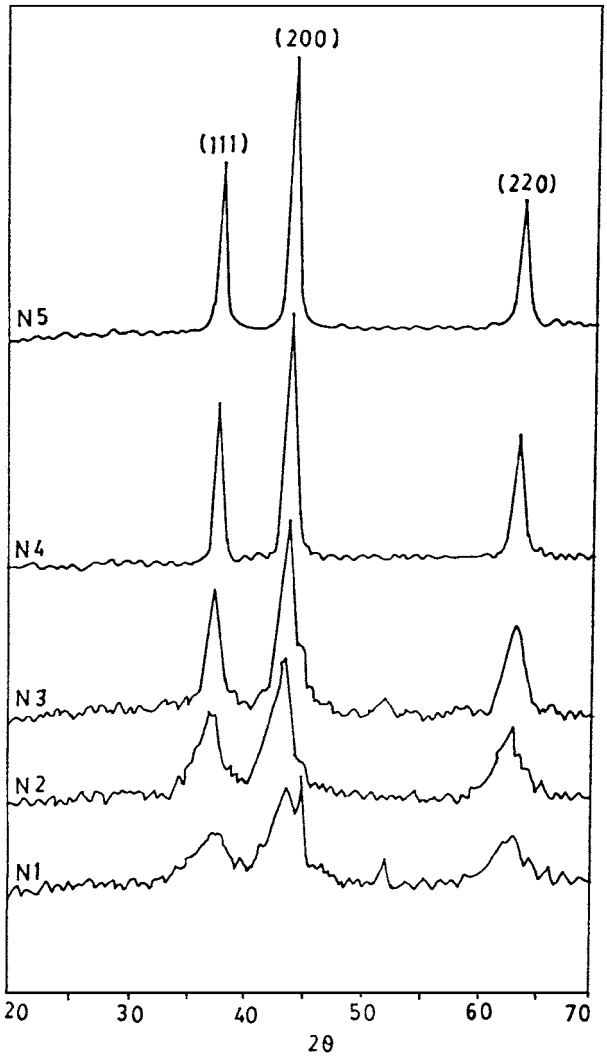

Figure 1 X-ray diffraction patterns of NiO nanoparticle samples.

90°C for 15 minutes in a hot air oven for electrode curing.

AC electrical measurements were carried out in an evacuated dielectric cell. Before taking the actual measurements, each pellet was subjected to a heat and cool run between 313 and 413 K in vacuum in order to remove any residual strain due to pelletisation. The complex impedance Z^* and the phase angle θ were measured at different signal frequencies ranging from 50 Hz to 3 MHz using a HIOKI Model 3531 Z-Hi Tester. The temperature of the sample pellets was varied from 313 to 413 K using an in-built heating system and electrical measurements were performed at an interval of 20 K, each temperature being kept constant with an accuracy of ± 1 K. The electrical measurements were limited to a maximum temperature of 413 K to avoid any

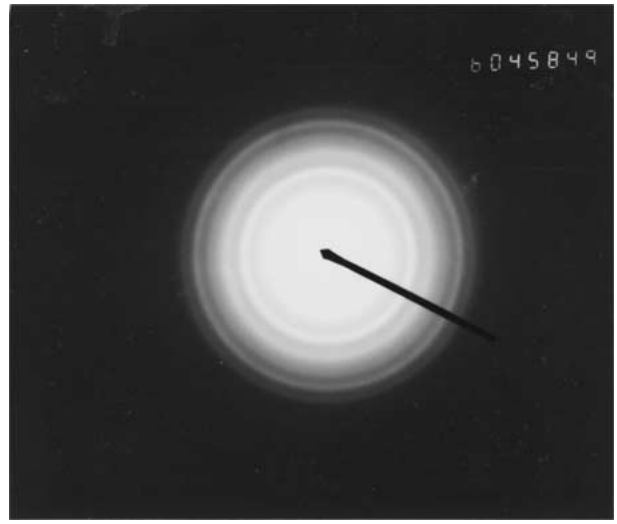

Figure 2 Electron diffraction pattern of the sample N1 having an average particle size of 2–3 nm.

grain growth of the particles and to ensure that the average size of the nanoparticles remained the same during the measurements. Sufficient stabilization time was ensured at each particular temperature. The repeatability of the readings was found to be good. Parallel equivalent circuit model was chosen for analyzing the data due to the high dielectric loss exhibited by the samples [41, 42].

3. Results and discussion

Electrical conductivity of nanoparticles of metals, alloys and semiconductors are reported to be markedly different from those of their single crystal and coarse-grained counterparts [1–11]. For metals like Cu, Pd, and Fe and alloys like $(Fe_{99}Cu_1)Si_9B_{13}$ and Ni-P, a decrease in conductivity was observed as the grain size was reduced to nanometer sizes [6]. In the case of semiconductor nanostructures, though the increase in the forbidden energy gap due to the narrowing of valence and conduction bands points to a possible decrease in conductivity, semiconductors like ZnS and CdS in the nanosize regime exhibit an increase in conductivity in comparison with their bulk counterparts [10].

In our earlier studies we have observed that the dc conductivity of consolidated nanoparticles of NiO σ_{DC} was enhanced by six to eight orders of magnitude over that of undoped NiO single crystals [38]. This enhancement in dc conductivity was attributed to the high concentration of Ni^{2+} vacancies (of the order of 10^{14} to 10^{16} cm^{-3}) associated with the defective grain boundary of NiO nanoparticles, which was estimated semi-quantitatively [38]. In the present study, the measured ac conductivity σ_m of NiO nanoparticles is found to be larger by six to eight orders of magnitude over that of NiO single crystals [12–28]. This is as expected since, though the charge transfer mechanisms in presence of dc and an ac fields are distinctly different in NiO, the charge carriers involved in both cases are holes associated with Ni^{2+} vacancies [12–15, 26–28]. The high density of Ni^{2+} vacancies explains the large enhancement in the ac conductivity of the order of six to eight in magnitude for the nanostructured samples in comparison with that of NiO single crystals.

Detailed discussions of the possible conductivity mechanisms in NiO are reported in the literature [12–37]. In undoped NiO, the conductivity is primarily associated with Ni^{2+} vacancies [12–37]. Each Ni^{2+} vacancy in the lattice causes the transformation of two adjacent Ni^{2+} ions into Ni^{3+} ions for acquiring charge neutrality and this transformation induces a local lattice distortion. The lowest possible energy state for this system consisting of one Ni^{2+} vacancy and two adjacent Ni^{3+} ions is that of a quadrupole complex [13, 15]. In NiO, at temperatures below 1000 K, the two holes associated with such a quadrupole complex contribute to conductivity by hopping and/ or by band like conduction depending on various parameters like temperature, frequency of the applied signal, defect concentration, and dopant concentration, if any [15]. The Correlated Barrier Hopping Model (CBH Model) has been successfully employed by many workers for analyzing the electrical conductivity data of a number of materials including NiO which exhibit defect dependent conductivity [26–29]. In the following discussion we present an analysis of the ac conductivity of consolidated nanoparticles of NiO as a function of frequency of the applied signal, temperature and average particle size based on the CBH model.

According to the CBH model, in NiO, the energy required for the hopping of holes from one Ni^{3+} site to Ni^{2+} site depends on a number of factors [28, 29]. At a single lattice site, a short range localization energy will arise because of the random fluctuations in site separation or atomic configurations or polaron effects [28, 29]. In addition, associated with each Ni^{2+} vacancy, there exists a long range defect potential well which affects the localization energy within a radius of a few lattice spacing [28, 29]. CBH model proposes two types of charge carrier movements in NiO as follows, [28, 29]

(i) Inter-well hopping involving the hopping of a hole from a Ni^{3+} ion located in one defect potential well to a Ni^{2+} ion in an adjacent defect potential well.
(ii) The hopping of holes between ions within one defect potential well constituting intra-well hopping.

In presence of a dc electric field, the probability of occurrence of intra-well hopping is zero and all the charge carriers (holes) in the material take part in inter-well hopping [28, 29]. Thus when a dc electrical field is applied, only the inter-well charge transfer process occurs resulting in pure dc conduction [28, 29]. However, in presence of an ac signal, both the aforementioned charge transfer mechanisms do have a finite probability of occurrence, their relative probabilities being dependent on the energy of the charge carriers, frequency of the applied signal, and concentration, mean site separation, depth and extend of percolation of the potential wells associated with Ni^{2+} vacancies [28, 29]. Thus the measured ac conductivity σ_m is constituted by a frequency independent dc component σ_{dc} (due to inter-well hopping) and a frequency dependent ac component σ_{ac} (due to intra-well hopping) i.e. $\sigma_m = \sigma_{dc} + \sigma_{ac}$ [28, 29]. It may be noted that the dc contribution to σ_m viz. σ_{dc} will be slightly less than the conductivity in presence of a dc field σ_{DC} since, even at very low frequencies of the applied ac signal (frequency $\rightarrow 0$) the probability of occurrence of intra-well hopping has a finite value and only a portion of the total number of charge carriers in the material take part in inter-well hopping.

In order to find the dc contribution (σ_{dc}) to the measured ac conductivity a two step curve fitting procedure devised by Jonscher was employed [43, 44]. In the first step nonlinear least square fitting was done on Y''–ω plots using the equation $Y'' = A_n(\omega)^n$ where $Y'' = \mathrm{Sin}\theta/|Z^*|$ is the imaginary part of the complex admittance function, A_n is a constant, $\omega = 2\pi f$ is the angular frequency of the applied ac signal and n (with $0 < n < 1$) is a measure of the deviation of the sample from ideal Debye behavior [43, 44]. In the second step nonlinear least square fitting was done on Y'–ω plots using the equation $Y' = [G_v + \omega^n A_n \mathrm{Cot}(n\pi/2)]$ using the values of A_n and n obtained from the first curve fitting procedure. Here $Y' = \mathrm{Cos}\,\theta/|Z^*|$ is the real part of the complex admittance function (measured ac conductance) and G_v is the pure dc contribution to Y'. From G_v values, σ_{dc} values were calculated knowing the dimensions of the pellets for all the samples. The results of curve fitting procedure for the sample N2 at 333 K are shown in Fig. 3 a and b.

The sample pellets used in the present study were dry pressed and were not sintered and hence some porosity may be present in them. Since, the samples were prepared by thermal decomposition of the carbonate precursor followed by annealing, the possibility of presence of pore fluids and adsorbed water is exceedingly small. The only possible moisture content should be that from air occluded during pelletisation. However, all the pellets were subjected to heat and cool runs between 313 and 413 K in vacuum before the electrical measurements and hence the moisture content and occluded air, if any, might almost completely be removed. Nan et al had reported that the contribution of pores to

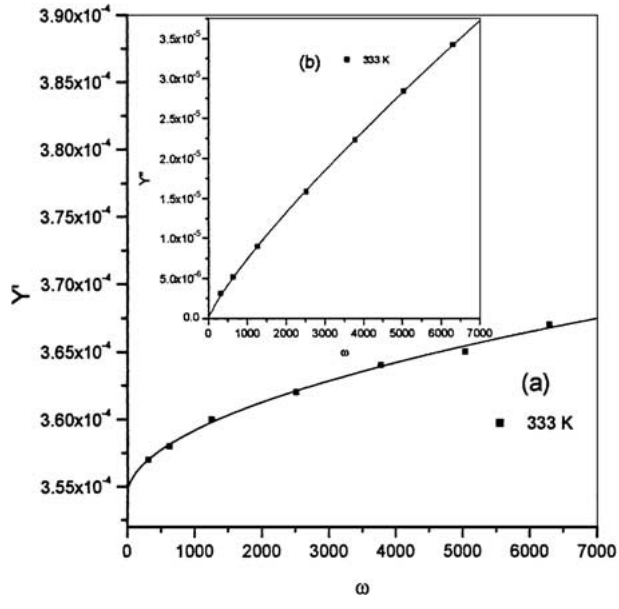

Figure 3 Results of curve fitting procedure for the sample N2 at 333 K (a) Y'–ω plot and (b) Y''–ω plot.

the ac electrical data will manifest as a low frequency semicircular arc in the complex Z'–Z'' plot with equivalent circuit parameters having the same temperature dependence as those for the high frequency semicircular arc representing the grain interior ac response [45]. This in turn means that the relaxation times corresponding to the electrical processes associated with the grain interior and porosity will have the same temperature dependence. In our earlier impedance spectroscopic study of nanostructured NiO samples, we had observed that the Z'–Z'' plots consist of two well resolved semicircular arcs—one at high frequencies and the other at low frequencies—with relaxation times exhibiting markedly different temperature dependences indicating that the low frequency semicircular arc is not associated with the pores [39]. We concluded that the contribution of pores to ac conductivity data of the nanostructured NiO samples, if at all any, is minimal.

3.1. Frequency dependence

The frequency dependence of the measured ac conductivity σ_m of the samples N1 and N2 at different temperatures are shown in Fig. 4. σ_m is found to be more or less independent of frequency below ≈50 kHz. A similar frequency independent response at low frequency region has earlier been reported for NiO thin films [26]. This low frequency region corresponds to the dc conductivity where the inter-well hopping responsible for pure dc conduction completely dominates over the intra-well hopping associated with pure ac conduction [26, 28–29]. At still higher frequencies, σ_m shows marked increase with frequency. A careful analysis of σ_m as the sum of σ_{dc} and σ_{ac} reveals the following general trends;

(i) At lower frequencies and higher temperatures (>373 K), σ_m is very nearly equal to σ_{dc} i.e. $\sigma_{ac} = \sigma_m - \sigma_{dc} \cong 0$ (Fig. 5). At lower frequencies and lower temperatures, σ_m is slightly higher than σ_{dc} and the contribution due to σ_{ac} is distinguishable.

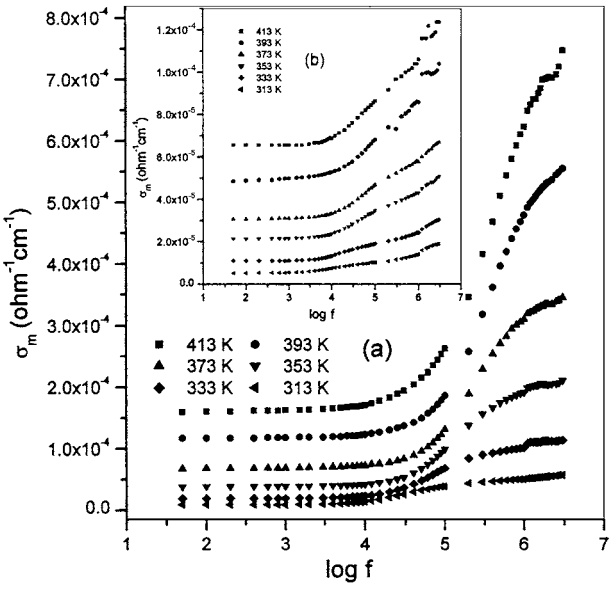

Figure 4 Frequency dependence of the measured ac conductivity σ_m at different temperatures for (a) sample N2 and (b) sample N1.

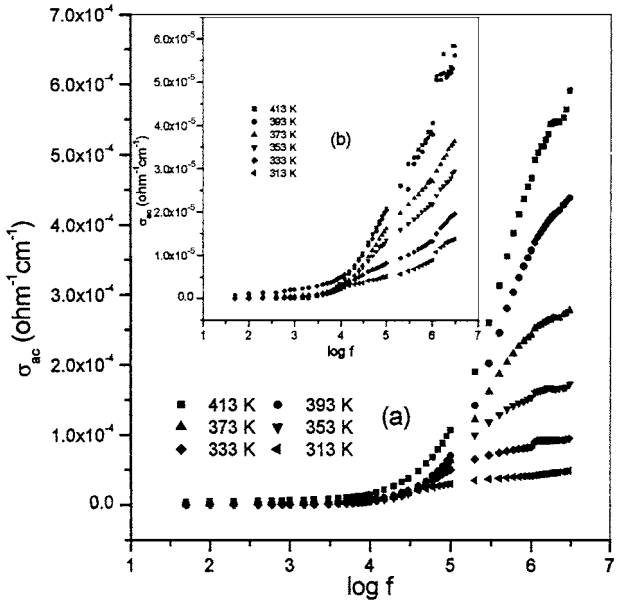

Figure 5 Frequency dependence of pure ac conductivity σ_{ac} for (a) sample N2 and (b) sample N1.

(ii) At higher frequencies and higher temperatures, the contribution of σ_{ac} to σ_m is more, though the contribution of σ_{dc} cannot be neglected. At higher frequencies and lower temperatures, σ_{ac} contribution to σ_m completely predominates over that due to σ_{dc}.

The variation of pure ac conductivity, $\sigma_{ac} = \sigma_m - \sigma_{dc}$ with frequency of the applied signal for the samples N1 and N2 are shown in Fig. 5.

At low frequencies the probability for inter-well hopping predominates over that due to intra-well hopping and $\sigma_m \approx \sigma_{dc}$ [28, 29]. The probability for inter-well charge transfer by hopping over the barrier (HOB) and hopping through the barrier (HTB) are given by [46]

$$W = W_0 \exp(-E_0/kT) \tag{1}$$

where E_0 is the activation energy for hopping, k the Boltzman constant and T the absolute temperature. The frequency factor, W_0, is given by

$$W_0 = (\pi/4kT E_0)^{1/2} J^2 h/2\pi,$$

for hopping through the barrier.

$$= \omega_0/2\pi, \quad \text{for hopping over the barrier.}$$

where J is the matrix element of the perturbing potential between hole wavefunctions centered at neighboring Ni^{2+} ions, h is the Plank's constant and ω_0 is the longitudinal optical phonon frequency [46]. From Equation 1 it is clear that the probability for both HOB and HTB increase as temperature is increased. Thus at higher temperatures and lower frequencies σ_m is dominated by inter-well hopping and σ_{ac} does not contribute to σ_m. However, as the signal frequency is increased to higher values, the probability of occurrence of intra-well hopping does increase and σ_{ac} contribute to σ_m [28, 29]. At lower temperatures the probability of occurrence of the inter-well charge transfer decreases

according to Equation 1 and even at low frequencies σ_{ac} contributes markedly to σ_m. At these lower temperatures, as the frequency of the applied signal is increased, the probability of occurrence of the intra-well hopping completely dominates over σ_{dc} (Figs 4 and 5). However, even at room temperature and in the MHz frequency range, σ_{dc} contributes markedly to σ_m which may be attributed to the percolation of the potential wells associated with Ni^{2+} vacancies [28, 29]. This is justifiable owing to the very high density of Ni^{2+} vacancies concentrated at the highly disordered and defective grain boundaries of the NiO nanoparticles [38, 47, 48].

An analysis of the frequency dependence of the pure ac conductivity, σ_{ac} in the form $\sigma_{ac} = A(\omega)^S$ was carried out. It was observed that 's' values are always less than 1 for all the samples at all temperatures. It was found that for all the five samples 's' values increased from 0.3 to 0.9 as the frequency increased from kHz to MHz range. In an earlier study by Lunkenheimer and Loidl on NiO thin films 's' values show some distribution (from 0.75 to 1.0) with frequency at temperatures above room temperature [26]. The wide distribution for 's' values with frequency observed in the present study of NiO nanoparticles might be a result of the random distribution of hoping distances and localization energies in the nanoparticle samples as discussed in Section 3.2 below.

3.2. Temperature dependence

The temperature dependence of σ_m of the samples at two selected frequencies are shown in Fig. 6a and b while this dependence for a typical sample N2 at different frequencies are shown in Fig. 7a. Arrhenius plots for the sample N2 at different frequencies is shown in Fig. 7b. Fig. 8a and b show the temperature dependence of pure ac conductivity, σ_{ac} of the samples at selected frequencies and Fig. 9a depicts the temperature dependence of σ_{ac} for the sample N2 at different frequencies and the corresponding Arrhenius plots are shown in Fig. 9b.

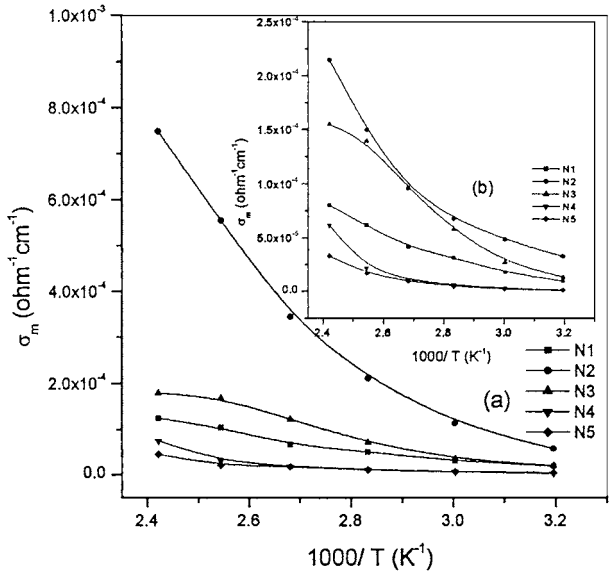

Figure 6 Temperature dependence of the measured ac conductivity σ_m for the samples at (a) 3 MHz and (b) 50 kHz.

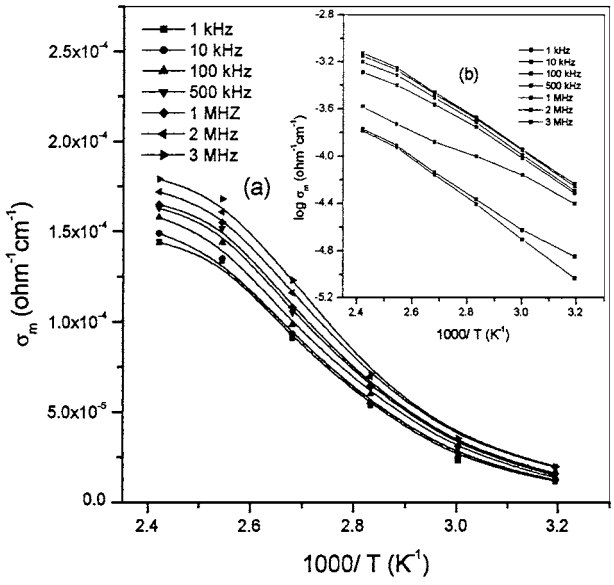

Figure 7 (a) Temperature dependence of the measured ac conductivity σ_m for the sample N2 at different frequencies and (b) corresponding Arrhenius plots.

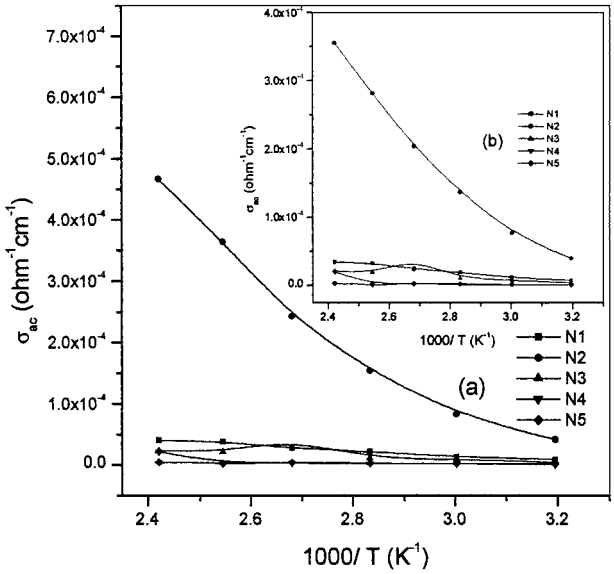

Figure 8 Temperature dependence of pure ac conductivity σ_{ac} for the samples at (a) 1 MHz and (b) 500 kHz.

An analysis of the results reveal that σ_m and σ_{ac} differ conspicuously in their temperature dependence, which is expected on the basis of the difference in the temperature dependence of the intra-well and inter-well charge transfer mechanisms [28, 29]. The activation energies for σ_m and σ_{ac} of the samples at different frequencies were calculated from Arrhenius plots and are listed in Table II. For comparison the activation energies for conductivity in presence of a dc electric field σ_{DC} (which is due to inter-well hopping alone) from our earlier studies is also included in the table [38]. It may be noted from Table II that the activation energy for σ_m is nearly equal to that for σ_{ac} in the MHz range, while at lower frequencies it is very close to that for σ_{dc}. This supports the inference that at MHz range σ_m is mostly contributed by intra-well hopping of charge carriers and at lower frequencies the major contribution to σ_m arises from inter-well hopping.

TABLE II Activation energies for σ_{DC}, σ_m and σ_{ac} calculated from Arrhenius plots

Sample code	σ_{DC} (eV)	Activation energy for σ_m (eV)					Activation energy for σ_{ac} (eV)				
		50 kHz	500 kHz	1 MHz	2 MHz	3 MHz	50 kHz	500 kHz	1 MHz	2 MHz	3 MHz
N1	0.30	0.24	0.23	0.23	0.21	0.20	0.14	0.18	0.18	0.15	0.16
N2	0.30	0.21	0.26	0.28	0.28	0.28	0.10	0.25	0.27	0.27	0.28
N3	0.30	0.29	0.28	0.28	0.26	0.26	0.18	0.19	0.18	0.15	0.17
N4	0.38	0.40	0.36	0.36	0.31	0.31	0.17	0.15	0.17	0.18	0.19
N5	0.40	0.39	0.33	0.33	0.27	0.27	0.14	0.14	0.14	0.16	0.16

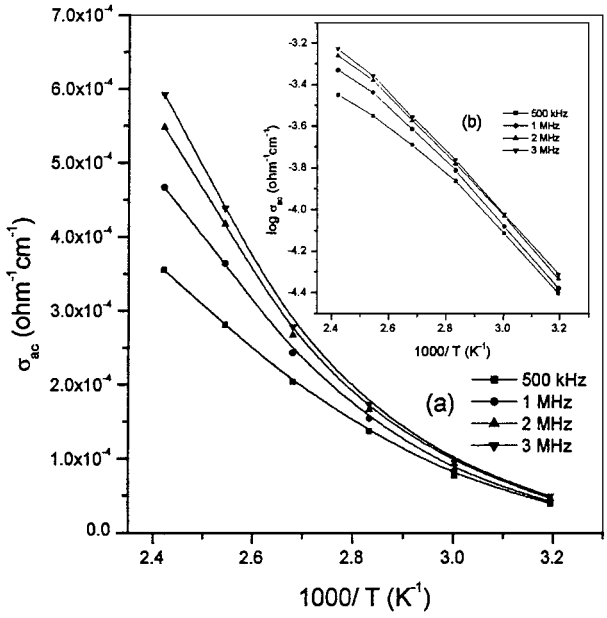

Figure 9 (a) Temperature dependence of pure ac conductivity σ_{ac} for the sample N2 at different frequencies and (b) corresponding Arrhenius plots.

The activation energy for the intra-well charge transfer (σ_{ac}) is determined by the short range localization energy, Δ, arising from the random fluctuations in the site separation of hopping sites and an energy $E(r)$ which depends on the position of the ions within the long range potential well associated with the Ni^{2+} vacancies [28, 29]. For intra-well hopping the average hopping distance is one lattice spacing [28, 29]. In the case of nanostructured materials, due to the high values for surface to volume ratio, a large percentage of the atoms reside in the grain boundary environment where the lattice parameter 'a' and hence the average hopping distance for intra-well hopping will have a distribution in value [6, 47, 48]. The activation energies calculated from Arrhenius plots represent only an average value of this quantity associated with the average hopping distance. The actual spread of lattice parameters in the samples will depend on a number of factors like the average grain size, ionic radii of the constituent ions, and shape of the grains. Qualitatively, we can say that the average hopping distance in the nanoparticles having different average particle sizes are nearly the same giving rise to nearly equal values for the activation energies obtained from Arrhenius plots. The diffused nature of the electron diffraction pattern (Fig. 2) is an indication of the structural disorder within the grain boundary of the nanoparticle sample. It may be inferred that the observed spread in 's' values for the samples in the present study also possibly arises from the spread in the hopping distance (lattice parameter) for the nanoparticle samples. According to Pollak and Pike $\sigma_{ac} \propto \omega^s$; $s \leq 1$ dependence occurs when the primitive relaxation times are exponential functions of one or more random variables with a reasonably smooth and wide distribution [49]. In the present case of NiO nanoparticles the random variables involved could be the hopping distance and the associated random fluctuations in the localization energy. It may be concluded that the observed spread in the 's' values and activation energies stem from the distribution in the numerical value of lattice parameter 'a', which is associated with the structure of the grain boundaries of the nanoparticle samples.

From Table II, it may be noted that the activation energies for σ_{ac} are smaller than those for σ_{dc}. This is attributable to the fact that for inter-well hopping corresponding to σ_{dc}, in addition to the short range localization energy, the long-range localization energy associated with the Ni^{2+} vacancies is to be overcome [28, 29]. The activation energy for σ_m should be the weighed average of the activation energies for σ_{ac} and σ_{dc}, weighed according to their relative probability of occurrence. From Table II, activation energy for σ_m falls in between that for σ_{ac} and σ_{dc}; at lower frequencies it is closer to that for σ_{dc} while at MHz range it approaches that for σ_{ac}. Also it may be noted that the activation energies for all the NiO nanoparticle samples in the present study are slightly less than that for NiO single crystals [15]. This can be attributed to the possible screening of charge carriers by the very high density of quadrupole complexes associated with the Ni^{2+} vacancies [15, 38].

3.3. Size dependence

Fig. 10a and b show the variation of measured ac conductivity σ_m with average particle size at different frequencies and different temperatures. It may be noted that σ_m increases as the average particle size increases from 2.5 nm for sample N1 to 4.5 nm for sample N2, tend to saturate and then falls off attaining a somewhat steady value for the samples N4 and N5 with larger average particle sizes. The variation has the same general form at different temperatures and frequencies. While Correlated Barrier Hopping may be considered to be the mechanism of charge transfer in the nanoparticle samples, the observed size dependence of σ_m can be explained on the basis of the variation of the structure

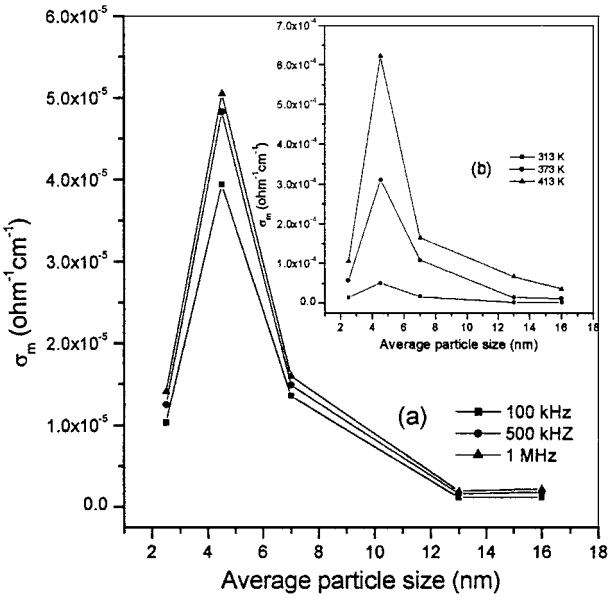

Figure 10 Variation of σ_m with average particle size (a) for different frequencies at 313 K and (b) for 1 MHz at different temperatures.

of the interfacial region as the size of the particles is changed.

In nanostructured materials, the structure and the volume fraction of the interfacial region have an important role in determining the transport properties [6, 38, 48, 50]. The interfacial region of nanostructured materials is composed of grain boundaries and triple junctions [6, 50]. Triple junctions which are intersection lines of three or more adjoining grains form a very important component of the interface along with grain boundaries in determining the transport properties as the grain size becomes smaller than about 10 nm [6, 50]. This is in sharp contrast with the case of coarse-grained samples where the effect of the triple junctions is negligible or altogether absent [50]. According to Bollman *et al*. triple junctions in nanostructured materials should be viewed as line defects which are analogous to dislocations [50, 51]. Hence the interfacial region of nanostructured materials can be pictured as constituting a potential barrier for the charge carriers with triple junctions corresponding to the maxima of the barrier [38, 50–52]. Earlier works on coarse-grained NiO samples, where the interfacial region is almost completely constituted by grain boundaries, have shown that the high density of Ni^{2+} vacancies associated with the grain boundaries enhances conductivity [13–15, 38]. However, the triple junctions in nanostructured NiO may justifiably have a reverse effect on conductivity. The physical basis for this assumption lies in the fact that the triple junction represents a maxima of a potential barrier and cause scattering of the charge carriers, resulting in a decreased rate of charge transport [6, 38, 50–52]. Thus, since the grain boundaries and triple junctions of nanostructured NiO has contrasting effects on conductivity, the value of σ_m for the nanoparticle samples having very small average particle size <10 nm will be determined by the relative volume fractions of the grain boundaries and triple junctions constituting the interfacial region. In the following semiquantitative analysis we present an explanation for the observed variation pattern of σ_m with average particle size on the basis of the variation of the volume fractions of the grain boundary (V_{gb}) and triple junctions(V_{tj}) with average particle size.

For nanocrystalline samples shapes such as a regular 14 sided tetrakaidecahedron for the grains is more realistic than spheres, cylinders, cubes etc and many earlier workers have employed this shape for calculating the interfacial volume fractions and the results from such calculations have been successfully complemented by experimental techniques such as small angle neutron scattering and positron annihilation spectroscopy [6, 38, 50, 51]. Further earlier crystallographic studies reports that the growth of NiO crystals occurs in tetrakaidecahedron shape [53]. An estimation of the volume fractions of the total interfacial region (V_{if}), grain boundary (V_{gb}) and triple junctions (V_{tj}) are carried out for the present samples assuming the grains to have a regular 14 sided tetrakaidecahedron shape with hexagonal faces representing grain boundaries and edges corresponding to triple junctions. The volume fractions are given by

$$V_{if} = 1 - [(d - D)/d]^3 \quad (2)$$

$$V_{gb} = [3D(d - D)^2]/d^3 \quad (3)$$

$$V_{tj} = [V_{if} - V_{gb}] \quad (4)$$

where d is the average particle size which is assumed to be the maximum diameter of an inscribed sphere and $D/2$ is the thickness of the interfacial region (outer skin of the tetrakaidecahedron) [6, 38, 50]. For all the calculations $D/2$ is assumed to be equal to 0.5 nm which is realistic in the size range of the particles in the present study [50, 54]. Fig. 11 shows the variation of V_{if}, V_{gb}, V_{tj} and $V_{gb} - V_{tj}$ with average particle size. The total interfacial region is maximum for the sample N1 with smallest average particle size (2.5 nm) and decreases

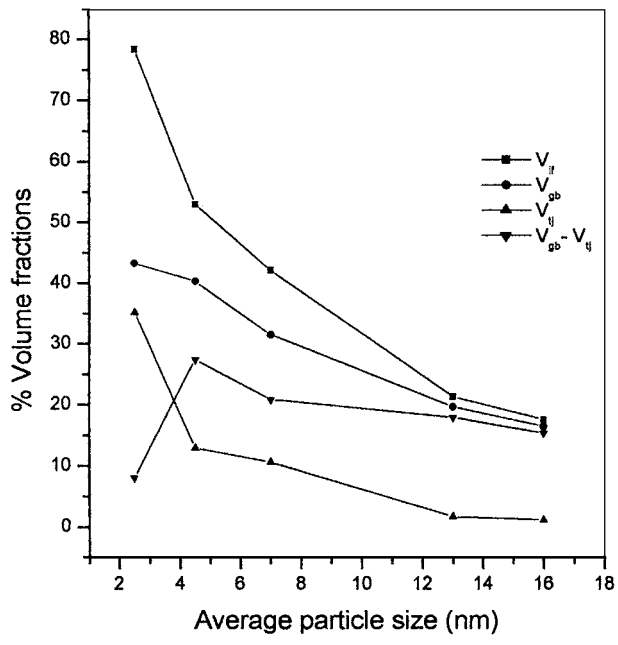

Figure 11 Variation of the calculated volume fractions of the total interfacial region (V_{if}), grain boundaries (V_{gb}), triple junctions (V_{tj}) and $V_{gb} - V_{tj}$ as a function of the average particle size.

gradually as the particle size increases to 16–17 nm for the sample N5. It may be clearly noted from Fig. 11 that although both V_{gb} and V_{tj} decreases as the particle size increases they do not exhibit the same pattern, whereas V_{gb} falls smoothly as the particle size is increased, V_{tj} falls sharply as the particle size increases from 2.5 nm for the sample N1 to 4.5 nm for the sample N2 and thereafter falls smoothly. For samples having larger average particle size V_{if}, V_{gb} and V_{tj} are almost independent of grain size and the volume fraction of the triple junctions constitutes only a very small portion of the total interfacial volume fraction (V_{if}). As explained earlier in this section the grain boundaries and triple junctions in nanocrystalline NiO have opposing effects on the conductivity and hence the conductivity should be proportional to the difference of the volume fractions, $V_{gb} - V_{tj}$. The variation of $V_{gb} - V_{tj}$ with particle size is shown in Fig. 11. This pattern is identical to the pattern in Fig. 10a and b and explains the observed variation of σ_m with average particle size. Thus it is emphasized that for nanostructured materials having very small average particle sizes (<10 nm), in addition to the grain boundaries, triple junctions become a very important constituent of the interfacial region in determining the transport properties. The dominant effect of the triple junctions is one of the important and interesting distinctions of nanostructured samples from coarse-grained polycrystalline samples having identical chemical composition.

4. Conclusion

NiO nanoparticle samples having different average particle sizes were prepared through a two step process. The ac conductivity of the nanoparticles consolidated in the form of pellets was studied as a function of frequency of the applied signal, temperature and average particle size. The observed enhancement in conductivity by six to eight orders of magnitude over that of NiO single crystals is attributed to the high defect density in nanostructured NiO. The measured ac conductivity σ_m was analyzed as the sum of pure ac component σ_{ac} and dc component σ_{dc}. The variation of σ_m and σ_{ac} with temperature and frequency of the applied signal and temperature are discussed on the basis of the Correlated Barrier Hopping (CBH) model. The variation of σ_m with average particle size is semi-quantitatively explained on the basis of the variation of $(V_{gb} - V_{tj})$ with particle size.

Acknowledgement

One of the authors V. Biju acknowledges Council of Scientific and Industrial Research (CSIR), Government of India for the financial support in the form of Senior Research Fellowship.

References

1. P. MARQUARDT, G. NIMTZ and B. MUHLSCHLEGEL, *Solid. Stat. Commun.* **65**(6) (1988) 539.
2. P. MARQUARDT, *Phys. Lett. A* (Netherlands) **123**(7) (1987) 365.
3. K. FRAHM, B. MUHLSCHLEGEL and R. NEMETH, *Z. Phys. B. Condens Mater.* **78**(1990) 91.
4. P. J. YETMAN and J. C. GILL, *Solid. Stat. Commun.* **62**(3) (1987) 201.
5. L. BRUS, *J. Phys. Chem.* **90**(1986) 2555.
6. C. SURYANARAYANA, *Bull. Mater. Sci.* **17**(4) (1994) 307.
7. Y. M. CHANG, E. B. LAVIK and D. A. BLOM, *Nanostruct. Mater.* **9**(1997) 633.
8. L. W. MOLENCAMP, H. VAN HOUTEN, A. A. M. STARING and C. W. J. BEENAKKER, *Physic. Scripta.* **T49**(1993) 441.
9. K. LU, J. T. WANG and W. D. WEI, *J. Phys. D. Appl. Phys.* **25** (1992) 808.
10. M. ABDUL KHADAR and B. THOMAS, *Nanostruct. Mater.* **10**(4) (1998) 593.
11. J. JOSE and M. ABDUL KHADAR, *ibid.* **11**(8) (1999) 1091.
12. W. J. MOORE, in "Seven Solid States" (W. A. Benjamin, New York, 1967) p. 133.
13. F. J. MORIN, *Phys. Rev. B.* **93**(6) (1954) 1199.
14. G. PARAVANO, *J. Chem. Phys.* **23**(1) (1955) 5.
15. D. ADLER and J. FEINLEIB, *Phys. Rev. B.* **2**(8) (1979) 3112.
16. P. PUSPHARAJAH and S. RADHAKRISHNA, *J. Mater. Sci.* **32** (1997) 3001.
17. Y. NAKUMARA, H. OGARA, T. NAKASHIMA, A. KISHIMOTO and H. YANAGIDA, *J. Amer. Ceram. Soc.* **80**(6) (1997) 1609.
18. YA. M. KSENDZOV, B. K. AVDEENKO and V. V. MAKAROV, *Sov. Phys. Solid. State.* **9**(4) (1967) 828.
19. A. J. BOSMAN and C. CREVECOEUR, *Phy. Rev.* **144**(2) (1965) 763.
20. S. KABASHIMA and T. KAWAKUBO, *J. Phys. Soc. Japan.* **24**(3) (1968) 493.
21. H. SATO, T. MINAMI, S. TAKATA and T. YAMADA, *Thin Solid Films* **236** (1993) 27.
22. S. VAN HOUTEN, *J. Phys. Chem. Solids.* **17**(1/2) (1960) 7.
23. M. A. KOLBER and R. K. MAC CORNE, *Phys. Rev. Lett.* **29**(21) (1972) 1457.
24. J. YAMASHITA and T. KUROSAWA, *J. Phys. Chem. Solids.* **5** (1958) 34.
25. R. R. HEIKES and W. D. JOHNSTON, *J. Chem. Phys.* **26**(3) (1957) 582.
26. P. LUNKENHEIMER, A. LOIDL, C. R. OTTERMANN and K. BANGE, *Phys. Rev. B.* **44**(11) (1991) 5927.
27. D. P. SNOWDEN and H. SALTSBURG, *Phys. Rev. Lett.* **14**(13) (1965) 497.
28. A. J. BOSMAN and H. J. VAN DAAL, *Adv. Phys.* **19**(77) (1970) 1.
29. M. SAYER, A. MANSINGH, J. B. WEBB and J. NOAD, *J. Phys. C. Solid. State. Phys.* **11** (1978) 315.
30. K. TERAKURA, A. R. WILLIAMS, T. OGUCHI and J. KUBLER, *Phys. Rev. Lett.* **52**(20) (1984) 1830.
31. G. K. WERTHEIN and S. HUFFNER, *ibid.* **28**(16) (1972) 1028.
32. J. ZAANEN, G. A. SAWATZKY and J. W. ALLEN, *ibid.* **55**[4] (1985) 418.
33. L. F. MATTHEISS, *Phys. Rev. B.* **5**(2) (1972) 290.
34. T. TAKAHASHI, *Ann. Phys.* **5**(3) (1996) 247.
35. V. V. MAKAROV, YA. M. KSENDZOV and V. I. KRUGLOV, *Sov. Phys. Solid. State.* **9**(2) (1967) 512.
36. J. E. KEEM, J. M. HONING and L. L. VAN ZANDT, *Philos. Mag. B.* **7**(2) (1973) 831.
37. W. E. SPEAR and D. S. TANNHAUSER, *Phys. Rev. B.* **7**(2) (1973) 831.
38. V. BIJU and M. ABDUL KHADAR, *Mater. Res. Bull.* **36**(1/2) (2001) 21.
39. *Idem., Mater. Sci. Eng. A* **304-306** (2001) 81.
40. A. TAYLOR, in "Xray Metallography" (Wiley, New York, 1961).
41. W. D. KINGERY, in "Introduction to Ceramics" (John Wiley and Sons, New York, 1986).
42. R. J. MAC DONALD, in "Impedance Spectroscopy: Emphasizing Solid Materials and Systems" (John Wiley & Sons, New York, 1987).
43. A. K. JONSCHER, *J. Mater. Sci.* **13** (1978) 553.
44. A. K. JONSCHER and J. M. REAU, *ibid.* **13** (1978) 563.
45. CE-WEN NAN, A. TSCHOPE, S. HOLTEN, H. KLIEM and R. BIRRINGER, *J. Appl. Phys.* **85**(11) (1999) 7735.

46. J. APPEL, *Phys. Rev. B.* **141**(2) (1966) 506.
47. H. J. WASSERMAN and J. S. VERMAAK, *Surf. Sci.* **22** (1970) 164.
48. R. BIRRINGER, *Mater. Sci. Eng. A.* **117** (1989) 33.
49. M. POLLAK and G. E. PIKE, *Phys. Rev. Lett.* **28**(22) (1972) 1449.
50. G. PALUMBO, S. J. THORPE and K. T. AUST, *Scr. Metal. Mater.* **22** (1990) 1347.
51. W. BOLLMAN, *Philos. Mag. A* **49**(1) (1984) 73.
52. E. Z. MEILIKHOV and R. M. FARZETDINOVA, *Physica E* **3** (1998) 190.
53. A. M. STONEHAM, *J. Phys. C. Solid. State. Phys.* **10** (1977) 1175.
54. CE-WEN NAN, XIAOPING LI, KEFENG CAI, JINZHANG TANG, *J. Mater. Sci. Lett.* **17** (1998) 1917.

Received 12 December 2000
and accepted 26 July 2001